This paper is available online at www.jbc.org

THE JOURNAL OF BIOLOGICAL CHEMISTRY VOL. 286, NO. 35, pp. 30258–30262, September 2, 2011


# Crystal Structure of Human ISG15 Protein in Complex with Influenza B Virus NS1B*[S]

Received for publication, May 4, 2011, and in revised form, June 30, 2011
Published, JBC Papers in Press, July 13, 2011, DOI 10.1074/jbc.C111.257899

**Liang Li[‡], Dongli Wang[‡], Yinan Jiang[‡], Jianfeng Sun[‡], Senyan Zhang[‡], Yuanyuan Chen[§], and Xinquan Wang[‡1]**

*From the [‡]Center for Structural Biology, Ministry of Education Key Laboratory of Protein Sciences, School of Life Sciences, Tsinghua University, Beijing 100084 and the [§]Institute of Biophysics, Chinese Academy of Sciences, Beijing 100101, China*

**ISG15 (interferon-stimulated gene 15), the first ubiquitin-like protein (UBL) identified, has emerged as an important cellular antiviral factor. It consists of two UBL domains with a short linker between them. The covalent attachment of ISG15 to host and viral proteins to modify their functions, similar to ubiquitylation, is named ISGylation. Influenza B virus NS1B protein antagonizes human but not mouse ISGylation because NS1B exhibits species specificity; it only binds human and non-human primate ISG15. Previous studies have demonstrated that the N-terminal UBL domain and linker of ISG15 are required for the binding by NS1B and that the linker plays a large role in the species specificity, but the structural basis for them has not been elucidated. Here we report the crystal structure of human ISG15 in complex with NS1B at a resolution of 2.0 Å. A loop in the ISG15 N-terminal UBL domain inserts into a pocket in the NS1B dimer, forming a high affinity binding site. The nonspecific van der Waals contacts around the ISG15 linker form a low affinity site for NS1B binding. However, sequence alignment reveals that residues in the high affinity site are highly conserved in primate and non-primate ISG15. We propose that the low affinity binding around the ISG15 linker is important for the initial contact with NS1B and that the stable complex formation is largely contributed by the following high affinity interactions between ISG15 N-terminal UBL domain and NS1B. This provides a structural basis for the species-specific binding of ISG15 by the NS1B protein.**

Type I interferon production represents one of the first lines of defense against invading viral pathogens (1, 2). Pathogens induce the expression of hundreds of interferon-stimulated genes (ISGs),[2] many of which help establish the antiviral responses in target cells (2, 3). One of the most prominent ISGs to be induced during viral infection and the ensuing type I interferon response is the ~15-kDa protein ISG15. It is a member of the ubiquitin-like (UBL) protein family, which is covalently attached to target proteins to modify their functions (4–6). As ISG15 modifies proteins in a manner similar to ubiquitylation, protein conjugation by ISG15 is termed ISGylation, and proteins are sequentially catalyzed by E1-activating enzyme Ube1L, E2-conjugating enzyme UbcH8, and E3 ligases such as human HerC5 and mouse HerC6 (5–7). ISG15 consists of two UBL domains linked by a short linker. Both domains share sequence and structural similarities to ubiquitin and are required for efficient conjugation of ISG15 to target proteins (8, 9).

ISG15 has recently emerged as an important cellular factor against different viral pathogens (10, 11). The antiviral activities associated with cellular and viral protein ISGylation *in vitro* and/or *in vivo* have been reported for both DNA and RNA viruses, including influenza A and B, Sindbis, herpes simplex virus type I (HSV-1), and murine γ herpesvirus 68 (γHV68) (12, 13). On the other side of the host-pathogen interaction, viruses evolve different mechanisms to escape from the antiviral activity of ISG15 (6, 10). Influenza B virus strongly induces ISG15 during infection but specifically blocks protein ISGylation by the NS1B protein, which interacts with ISG15 and inhibits its conjugation to target proteins *in vitro* as well as in infected cells (14). The binding site for human ISG15 is located in the N-terminal 103 residues of NS1B (14). The NS1B protein also exhibits species-specific binding; it binds ISG15 from human and non-human primates but not from other mammalian species including mouse and dog (7, 15). It has been shown that the N-terminal UBL domain and linker region in human ISG15 are important for NS1B binding (7, 15). There are residues in the ISG15 linker region that are highly conserved among primates but divergent in other mammalian species (15). Substitution of these residues in human ISG15 with corresponding mouse residues abolished its binding with NS1B (15). Although previous studies have provided invaluable information (7, 14–16), the complex structure of human ISG15 with NS1B is still needed to definitively elucidate the structural basis for the binding and its species specificity. Here we report the crystal structure of the full-length human ISG15 in complex with the N-terminal 103 residues of NS1B.

## EXPERIMENTAL PROCEDURES

*Protein Expression and Purification*—All constructs expressing the NS1B N-terminal fragment, human ISG15, and its mutants were generated using a standard PCR-based cloning strategy. Recombinant full-length human ISG15 (1–158) with a C78S mutation and a C-terminal arginine cap was expressed with the pGEX-6P-1 vector in *Escherichia coli* strain BL21 (DE3). ISG15 and its mutants with an N-terminal glutathione *S*-transferase (GST) tag were collected with glutathione-Sepharose 4 Fast Flow (GE Healthcare) followed by digestion with PreScission protease (GE Healthcare) to remove the tag and

* This work was supported by grants from the Ministry of Science and Technology (Grants 2011CB910502 and 2010CB912402), the Ministry of Education of China (Grants 20090002120036 and 20100002110001), the Tsinghua University 985 Phase II fund, and the Fok Ying Tung Education Foundation.

*The atomic coordinates and structure factors (code 3RT3) have been deposited in the Protein Data Bank, Research Collaboratory for Structural Bioinformatics, Rutgers University, New Brunswick, NJ (http://www.rcsb.org/).*

[S] The on-line version of this article (available at http://www.jbc.org) contains supplemental Table S1 and Figs. S1–S5.

[1] To whom correspondence should be addressed: Medical Science Bldg. C226, Tsinghua University, Beijing 100084, China. Tel.: 86-10-62789401; E-mail: xinquanwang@mail.tsinghua.edu.cn.

[2] The abbreviations used are: ISG, interferon-stimulated gene; UBL, ubiquitin-like protein; SPR, surface plasmon resonance; RBD, RNA-binding domain; r.m.s., root mean square.

further purification by Superdex 200 HR 10/30 gel filtration (GE Healthcare). The N-terminal fragment of NS1B (residues 1–103) was expressed with the pET-22b vector in *E. coli* BL21 (DE3). NS1B with a C-terminal $His_6$ tag was purified using nickel-nitrilotriacetic acid affinity resin (Qiagen) followed by Superdex 200 HR 10/30 gel filtration (GE Healthcare). The purified ISG15 and NS1B were incubated on ice for 30 min, and the stable ISG15-NS1B complex was further purified by Superdex 200 HR 10/30 gel filtration (GE Healthcare).

*Crystal Growth*—The ISG15-NS1B complex in the buffer containing 0.01 M HEPES, pH 7.2, 0.5 M NaCl was concentrated to ~20 mg/ml for initial screening of crystallization conditions. Crystals were grown at 18 °C by the sitting drop vapor diffusion method, using equal volumes of protein and crystallization solution over a 0.6-ml reservoir composed of 20% PEG 8000, 0.1 M HEPES, pH 7.5, 0.01 M succinic acid. Crystals were cryoprotected in well solution plus 20% (v/v) glycerol and then flash-frozen in the liquid nitrogen before data collection.

*Data Collection and Structural Determination*—A 2.0 Å dataset was collected on beamline BL17U at the Shanghai Synchrotron Research Facility (SSRF) and processed with HKL2000 (17). The structure was determined by the molecular replacement method with human ISG15 structure (Protein Data Bank (PDB) code: 1Z2M) (8) and NS1B structure (PDB code: 1XEQ) (18) as search models in the program PHASER (19). Iterative refinement and model building were conducted with the programs PHENIX (20) and COOT (21), respectively. All structural figures were made with PyMOL (22).

*Gel Filtration Analysis*—Size-exclusion chromatography with a Superdex 200 10/300 column on an ÄKTA FPLC (GE Healthcare) was carried out to access the apparent molecular mass of the ISG15-NS1B complex in solution at 4 °C. The column was equilibrated with a buffer containing 0.01 M HEPES, pH 7.2, 0.15 M NaCl at a flow rate of 0.5 ml/min. The ISG15-NS1B complex with a starting concentration of ~10 mg/ml (0.5-ml volume) was loaded to the column, and fractions of 0.5 ml each were collected. The fraction corresponding to the peak of the ISG15-NS1B complex elution (0.5 -ml volume) was loaded again to the column. The same analysis was performed two more times until the $UV_{280}$ absorbance of the peak went down to ~20 milliabsorbance units. Aliquots of fractions from all four gel filtration analyses were subjected to SDS-polyacrylamide gel electrophoresis (PAGE), and proteins were visualized by Coomassie Blue staining. The column was calibrated with molecular mass standards.

*BIAcore Analysis*—Real-time binding and the following analysis by surface plasmon resonance (SPR) were carried out on a BIAcore T100 instrument (GE Healthcare) at 25 °C. The NS1B protein was immobilized on a research-grade CM5 sensor chip by the amine-coupling method. Flow cell 1 was left blank as a reference. NS1B (10 μg/ml) in sodium acetate buffer (10 mM, pH 5.0) was immobilized to 300–400 response units on the flow cell, and the surface was then blocked with an injection of 1 M ethanolamine, pH 8.0, for 7 min. An injection of 10 mM NaOH for 10 s was carried out to remove non-covalently bound NS1B. For the collection of data for kinetic or equilibrium analyses, ISG15 and all its mutants in a buffer of 0.01 M HEPES, pH 7.2, and 0.5 M NaCl, plus 0.005% (v/v) Tween 20, were injected over the flow cells at various concentrations at a 30 μl/min flow rate. The ISG15-NS1B complex was allowed to associate for 60 s and dissociate for 120 s. Data were analyzed with the BIAcore T100 evaluation software by fitting to a 1:1 Langmuir binding fitting model.

**TABLE 1**
**Data collection and refinement statistics**

| | |
|---|---|
| **Data collection** | |
| Beamline | SSRF BL17U |
| Wavelength | 0.9793 |
| Space group | C2 |
| Cell dimensions | |
| *a*, *b*, *c* (Å) | 93.68, 39.15, 74.70 |
| α, β, γ (°) | 90, 90.5, 90 |
| Resolution (Å) | 50-2.00 (2.05-2.00)[a] |
| $R_{merge}$ (%) | 12.0 (32.3) |
| $I/\sigma I$ | 14.4 (3.0) |
| Completeness (%) | 91.5 (86.2) |
| Redundancy | 4.0 (2.5) |
| **Refinement** | |
| Resolution (Å) | 46.8-2.00 |
| No. of reflections | 16316 |
| $R_{work}/R_{free}$ (%) | 18.9/24.3 |
| No. of atoms | |
| Protein | 1950 |
| Water | 85 |
| Succinic acid | 2 |
| *B*-factors (Å$^2$) | |
| Protein | 40.7 |
| Water | 42.6 |
| Succinic acid | 68.9 |
| r.m.s. deviations | |
| Bond lengths (Å) | 0.007 |
| Bond angles (°) | 1.045 |
| Ramachandran plot | |
| Most favored | 93.9 |
| Additionally allowed | 6.1 |
| Generously allowed | 0.0 |
| Disallowed | 0.0 |

[a] Values in parentheses are for highest resolution shell.

## RESULTS AND DISCUSSION

The ISG15-NS1B complex structure was determined by the molecular replacement method and refined at 2.0 Å with a final $R_{work}$ and $R_{free}$ of 18.9 and 24.3%, respectively (Table 1). The asymmetric unit contains one NS1B molecule and one ISG15 molecule (Fig. 1*A*). By applying symmetrical operation, two NS1B monomers (A and B) form a closely packed homodimeric six-helix fold (Fig. 1*B*), which has the same architecture as unbound NS1B dimer structure previously determined (supplemental Fig. S1*A*) (18). The NS1B dimer binds two ISG15 molecules symmetrically (Fig. 1*B*). The gel filtration analysis showed that the NS1B exists as dimer (molecular mass 25.4 kDa) in solution (Fig. 1*C*). To examine the binding stoichiometry of the NS1B dimer with ISG15 in solution, we performed gel filtration analyses of the ISG15-NS1B complex four times from high to low protein concentration, which was facilitated by repeatedly loading the peak fraction of previous ISG15-NS1B elution to the column. With a starting concentration of ~10 mg/ml, the peak volume of the ISG15-NS1B complex is 14.9 ml (Fig. 1*C*) in the first run. The elution volume of the ISG15-NS1B complex decreased to 15.3 and 15.7 ml in the second and third run (Fig. 1*C*). In the fourth run, the peak volume did not decrease and remained to be 15.7 ml (Fig. 1*C*). The molecular mass standards BSA (66 kDa) and ovalbumin (44 kDa) have peak volumes of 14.6 and 15.7 ml, respectively, indicating that the molecular mass of the ISG15-NS1B complex changed from close to 66 to 44 kDa with decreased protein

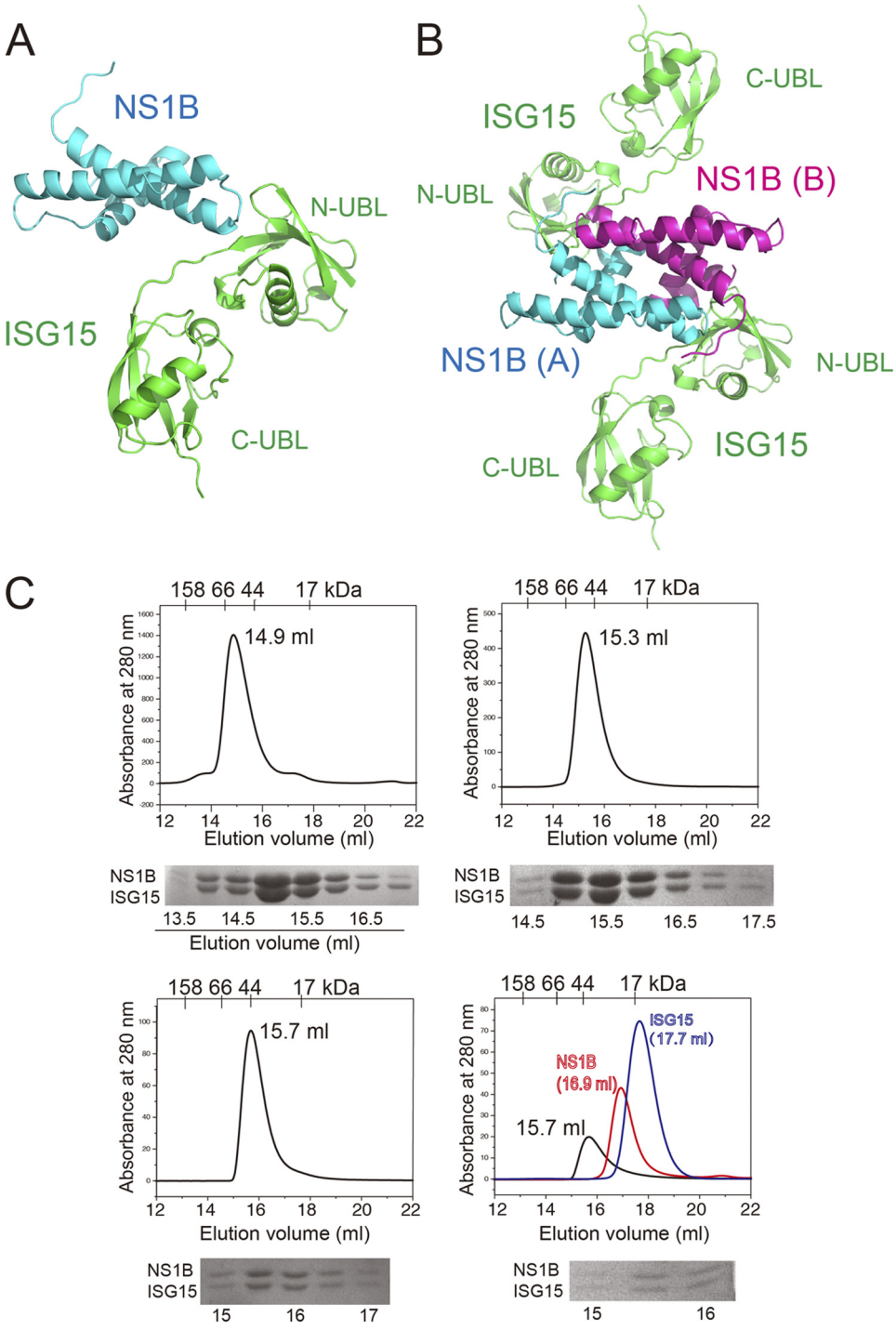


FIGURE 1. **Structure of the ISG15-NS1B complex and gel filtration analysis in solution.** *A*, ribbon diagram of one NS1B molecule (*cyan*) and one ISG15 molecule (*green*) in the asymmetric unit. *N-UBL*, N-terminal UBL; *C-UBL*, C-terminal UBL. *B*, the NS1B dimer (monomers A and B colored with *cyan* and *magenta*, respectively) bound with two ISG15 molecules after applying the symmetrical operation. *C*, gel filtration analyses of the ISG15-NS1B complex in solution. The *top left panel* shows the gel filtration profile after an injection of 0.5 ml of ISG15-NS1B complex (~10 mg/ml). The *top right panel* shows the gel filtration profile of the second run after injecting the peak fraction (0.5 ml) from the first run. The *bottom left panel* shows the gel filtration profile of the third run after injecting the peak fraction (0.5 ml) from the second run. The *bottom right panel* shows the gel filtration profile of the fourth run after injecting the peak fraction (0.5 ml) from the third run (*black curve*). The elution volumes of the NS1B dimer (*red curve*, molecular mass 25.4 kDa) and ISG15 monomer (*blue curve*, molecular mass 17.7 kDa) are 16.9 and 17.7 ml, respectively. In all 15% SDS-PAGE gels showing the components of the ISG15-NS1B complex elution, the NS1B monomer (12.7 kDa) migrated slower than ISG15 (17.7 kDa), which was further confirmed by peptide mass fingerprinting after enzymatic digestion of both bands.

concentration. The calculated molecular mass of the NS1B dimer bound with two ISG15 molecules including extra residues after PreScission cleavage and $His_6$ tag is 60.8 kDa. The calculated molecular mass of the NS1B dimer bound with one ISG15 molecule is 43.1 kDa. These results collectively indicate that in solution, the NS1B dimer may bind two copies or one copy of ISG15, depending on the protein concentration.

The overall structure of the NS1B monomer did not change substantially upon binding ISG15 when compared with

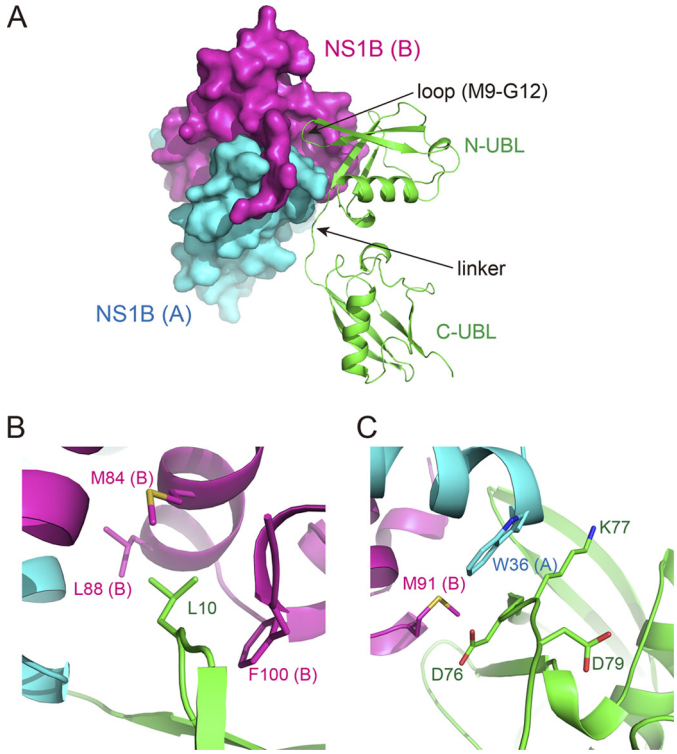


FIGURE 2. **The binding interface in the ISG15-NS1B complex.** *A*, overall view of the binding interface. The NS1B dimer is shown in surface representation. One binding site is around the Met-9–Gly-12 loop in ISG15. Another binding site is around the linker connecting the N-terminal UBL (*N-UBL*) and C-terminal UBL (C-UBL) in ISG15. *B*, ISG15 residue Leu-10 in the N-terminal UBL domain and surrounding interacting residues of NS1B in the pocket. Residues from NS1B monomer A and monomer B are labeled in *parentheses*. *C*, ISG15 residues Asp-76 and Lys-77 in the linker have van der Waals contacts with Met-91 and Trp-36 of NS1B.

unbound NS1B monomer (18), with an r.m.s. deviation of 0.58 Å for Cα atoms (residues 9–90). However, there is a large conformational change of the C-terminal tail (residues 91–103) of NS1B in the complex to facilitate interactions with ISG15, which will be described below (supplemental Fig. S1*B*). The overall structure of ISG15, consisting of N- and C-terminal UBL domains and the linker between them, also did not change substantially upon binding NS1B when compared with free ISG15 (supplemental Fig. S1*C*) (8). The r.m.s. deviation for 152 Cα atoms is ~0.82 Å. The N-terminal UBL domain and the following linker region of ISG15 have contact with the NS1B dimer in the complex (Fig. 1*B*), and the C-terminal UBL domain of ISG15 is away from the NS1B dimer without any interaction (Fig. 1*B*). This is consistent with previous studies showing the importance of the N-terminal UBL domain and linker region of human ISG15 in NS1B binding (7, 15).

Because the two binding interfaces between the NS1B dimer and two ISG15 molecules in the crystal structure are identical, we only analyze one interface in the following description and discussion. At the binding interface, a protruding loop (Met-9–Gly-12) from the ISG15 N-terminal UBL domain inserts into a pocket contributed by both NS1B monomers (Fig. 2*A*). At a 4 Å distance cutoff, residues Met-9, Leu-10, Ala-11, and Gly-12 from this loop have extensive interactions with residues Gln-37 and Ala-39 from NS1B monomer A and residues Ala-19, Met-84, Leu-88, Gly-99, Phe-100, and Pro-102 from NS1B monomer B (supplemental Table S1). The overall property of interactions in the pocket is hydrophobic. ISG15 residue Leu-10 is the central interacting residue in the pocket, which has interactions with Met-84, Leu-88, and Phe-100 of the NS1B monomer B and contributes to nearly 20% of the total buried surface upon complex formation (Fig. 2*B* and supplemental Fig. S2*A*). Mutation of this residue (L10A) decreased the binding affinity with NS1B from 0.18 to 50 μM (Table 2 and supplemental Fig. S3). Other hydrophobic residues including Ile-36, Leu-72, Leu-73, Val-74, and Val-75 in the ISG15 N-terminal UBL domain also have contacts with NS1B at the binding interface (supplemental Table S1).

**TABLE 2**
**Affinities of ISG15 wild type and its mutants binding to immobilized NS1B**

All measurements were performed two independent times except for ISG15 D76Q/K77N/D79S mutant.

| | Fit model | $k_{on}$ (mean ± S.D.) | $k_{off}$ (mean ± S.D.) | $K_D$ (mean ± S.D.) |
|---|---|---|---|---|
| | | $M^{-1}s^{-1} \times 10^5$ | $s^{-1} \times 10^{-2}$ | μM |
| WT | Kinetics | 1.6 ± 0.1 | 3.0 ± 0.2 | 0.18 ± 0.01 |
| L10A | Steady state | | | 50 ± 13 |
| D76Q | Steady state | | | 6.2 ± 2.3 |
| K77N | Steady state | | | 1.7 ± 0.6 |
| D79S | Kinetics | 2.2 ± 1.0 | 4.0 ± 0.2 | 0.20 ± 0.10 |
| D76Q/K77N/D79S | Steady state | | | 5.2 |

The previously identified critical linker region (Asp-76–Asp-79) contacts the NS1B dimer at the binding interface (Fig. 2*A*) (7, 15). Replacing residues Asp-76, Lys-77, and Asp-79 in human ISG15 with corresponding mouse residues Gln, Asn, and Ser abolished the binding with NS1B in GST pulldown assay (15). At a 4 Å distance cutoff, residues Asp-76 and Lys-77 from ISG15 have contacts with Met-91 from NS1B monomer A and Trp-36 from NS1B monomer B (Fig. 2*C* and supplemental Fig. S2*B*). The interactions are characterized by the van der Waals packing of side chains without specific hydrogen-bonding or salt bridge interactions (Fig. 2*C*). Residue Asp-79 does not interact with any NS1B residues (Fig. 2*C*). Our SPR analysis supports the structural characteristics, showing that single D76Q and K77N mutations decreased the NS1B binding affinity from 0.18 μM to 6.2 and 1.7 μM, respectively (Table 2 and supplemental Fig. S3). Mutant D79S still had a binding affinity of 0.20 μM, which is close to that of wild type ISG15 (0.18 μM) (Table 2 and supplemental Fig. S3). We also made a human ISG15 with a D76Q/K77N/D79S triple mutation, which induced the same level of affinity decrease (5.2 μM) as the single D76Q mutation (Table 2 and supplemental Fig. S3).

In the ISG15-NS1B complex, the NS1B 1–103 fragment consists of three helices (α1, α2, and α3), two connecting loops (L1 and L2), and the N- and C-terminal tails (supplemental Fig. S4*A*). When compared with unbound NS1B, the C-terminal tail of NS1B in the complex has a close to 180° degree rotation (supplemental Fig. S1*B*), enabling residues on it to interact with ISG15. Among the 15 ISG15-interacting residues on NS1B, seven of them are located in the C-terminal tail including Met-91, Pro-93, Ser-94, Ile-97, Gly-99, Phe-100, and Gly-101 (supplemental Table S1), and Met-91 and Phe-100 are extensively involved in the hydrophobic interactions with the protruding ISG15 loop (Met-9–Gly-12) in the pocket (Fig. 2*B*). This explains the previous observation that both the RNA-binding domain (RBD, the N-terminal 93 residues) and the 94–103

region of NS1B are required for ISG15 binding (14). The NS1B RBD (residues 1–93) and corresponding influenza virus A NS1A RBD (1–73) share a similar homodimeric six-helix fold (18). In the architecture, six helices α1, α2, α3, α1′, α2′, and α3′ are conserved in both length and position, whereas the L2 loop is eight amino acids longer in NS1B (supplemental Fig. S4*A*). The unique Arg-38–Arg-38 pair and two Arg-35–Arg-46 pairs in the NS1A RBD dimer for dsRNA binding are strictly conserved in the NS1B RBD (supplemental Fig. S4*A*) (23), indicating that the NS1B RBD binds dsRNA similarly as the NS1A RBD. The ISG15 and dsRNA binding sites are on different sides of the NS1B dimer, which is consistent with a previous study showing that dsRNA and ISG15 can bind to NS1B simultaneously (supplemental Fig. S5) (16).

Our mutagenesis and SPR analysis showed that mutation of Leu-10 in the ISG15 N-terminal UBL domain decreased the NS1B binding affinity close to 300-fold (Table 2), whereas mutation of residues in the ISG15 linker decreased the NS1B binding affinity 10–30-fold (Table 2). This indicates that the binding around the ISG15 linker by NS1B is weaker than the binding around the ISG15 N-terminal UBL domain by NS1B. However, the ISG15 linker plays a very significant role in the species-specific binding by NS1B (15). Sequence alignment shows that hydrophobic ISG15 residues Met-9, Ile-10, Ile-36, Leu-72, Leu-73, Val-74, and Val-75 forming the high affinity binding site on the N-terminal UBL domain are highly conserved among primates and non-primates (supplemental Fig. S4*B*). Therefore, most probably the N-terminal UBL domain would not determine the species-specific binding by NS1B. These observations lead us to speculate that although the binding around the ISG15 linker by NS1B is relatively weak, it may provide contact to bring NS1B and ISG15 close, and then the high affinity binding between the ISG15 N-terminal UBL domain and NS1B may provide the following extensive interactions for stable complex formation. In this binding model, the initial contact of NS1B with the linker region of ISG15 is critical not only for bringing these two molecules close but also for positioning them in the appropriate orientation to facilitate extensive interactions between the ISG15 N-terminal UBL domain and NS1B. This also provides a structural basis for the species-specific binding of ISG15 by NS1B.

The ISG15 C-terminal UBL has a C-terminal conserved LRLRGG motif that is covalently linked to target proteins (supplemental Fig. S4*B*). The ovarian tumor (OTU) domain proteases encoded by nairoviruses and arteriviruses help counteract both ubiquitylation and ISGylation by cleaving ubiquitin and ISG15 from target proteins (24). Structural studies showed that the ovarian tumor protease binds to the ubiquitin and C-terminal UBL domain of ISG15 (25, 26). Previous biochemical study and the ISG15-NS1B complex structure shown here reveal that NS1B just targets the N-terminal UBL domain and the linker of ISG15 (9). It supports the previous proposal that the N-terminal UBL domain of ISG15 mainly functions in the ligation step of ISGylation and that NS1B inhibits ISGylation by competing with E3 ligase for binding to the N-terminal UBL domain (9).

*Acknowledgments—We thank J. H. He, S. Huang, and L. Tang at SSRF beamline BL17U for assistance with data collection and J. W. Wang, J. W. Wu, and H. T. Li for discussion.*

*Addendum*—While this manuscript was under review, the crystal structure of human ISG15 in complex with NS1B (PDB code: 3R66) determined by R. Guan, L. C. Ma, R. M. Krug, and G. T. Montelione at the Northeast Structural Genomics Consortium was released from the PDB. This structure is in space group P1 and has one NS1B dimer bound with two ISG15 molecules in the asymmetric unit.

## REFERENCES

1. Borden, E. C., Sen, G. C., Uze, G., Silverman, R. H., Ransohoff, R. M., Foster, G. R., and Stark, G. R. (2007) *Nat. Rev. Drug Discov.* **6,** 975–990
2. Randall, R. E., and Goodbourn, S. (2008) *J. Gen. Virol.* **89,** 1–47
3. Sadler, A. J., and Williams, B. R. (2008) *Nat. Rev. Immunol.* **8,** 559–568
4. Loeb, K. R., and Haas, A. L. (1992) *J. Biol. Chem.* **267,** 7806–7813
5. Zhang, D., and Zhang, D. E. (2011) *J. Interferon Cytokine Res.* **31,** 119–130
6. Jeon, Y. J., Yoo, H. M., and Chung, C. H. (2010) *Biochim. Biophys. Acta* **1802,** 485–496
7. Versteeg, G. A., Hale, B. G., van Boheemen, S., Wolff, T., Lenschow, D. J., and García-Sastre, A. (2010) *J. Virol.* **84,** 5423–5430
8. Narasimhan, J., Wang, M., Fu, Z., Klein, J. M., Haas, A. L., and Kim, J. J. (2005) *J. Biol. Chem.* **280,** 27356–27365
9. Chang, Y. G., Yan, X. Z., Xie, Y. Y., Gao, X. C., Song, A. X., Zhang, D. E., and Hu, H. Y. (2008) *J. Biol. Chem.* **283,** 13370–13377
10. Harty, R. N., Pitha, P. M., and Okumura, A. (2009) *J. Innate Immun.* **1,** 397–404
11. Skaug, B., and Chen, Z. J. (2010) *Cell* **143,** 187–190
12. Lenschow, D. J., Giannakopoulos, N. V., Gunn, L. J., Johnston, C., O'Guin, A. K., Schmidt, R. E., Levine, B., and Virgin, H. W., 4th (2005) *J. Virol.* **79,** 13974–13983
13. Lenschow, D. J., Lai, C., Frias-Staheli, N., Giannakopoulos, N. V., Lutz, A., Wolff, T., Osiak, A., Levine, B., Schmidt, R. E., García-Sastre, A., Leib, D. A., Pekosz, A., Knobeloch, K. P., Horak, I., and Virgin, H. W., 4th (2007) *Proc. Natl. Acad. Sci. U.S.A.* **104,** 1371–1376
14. Yuan, W., and Krug, R. M. (2001) *EMBO J.* **20,** 362–371
15. Sridharan, H., Zhao, C., and Krug, R. M. (2010) *J. Biol. Chem.* **285,** 7852–7856
16. Yuan, W., Aramini, J. M., Montelione, G. T., and Krug, R. M. (2002) *Virology* **304,** 291–301
17. Otwinowski, Z., Borek, D., Majewski, W., and Minor, W. (2003) *Acta Crystallogr. A* **59,** 228–234
18. Yin, C., Khan, J. A., Swapna, G. V., Ertekin, A., Krug, R. M., Tong, L., and Montelione, G. T. (2007) *J. Biol. Chem.* **282,** 20584–20592
19. McCoy, A. J., Grosse-Kunstleve, R. W., Adams, P. D., Winn, M. D., Storoni, L. C., and Read, R. J. (2007) *J. Appl. Crystallogr.* **40,** 658–674
20. Adams, P. D., Grosse-Kunstleve, R. W., Hung, L. W., Ioerger, T. R., McCoy, A. J., Moriarty, N. W., Read, R. J., Sacchettini, J. C., Sauter, N. K., and Terwilliger, T. C. (2002) *Acta Crystallogr. D Biol. Crystallogr.* **58,** 1948–1954
21. Emsley, P., and Cowtan, K. (2004) *Acta Crystallogr. D Biol. Crystallogr.* **60,** 2126–2132
22. DeLano, W. L. (2010) *The PyMOL Molecular Graphics System*, version 1.3r1, Schrödinger, LLC, New York
23. Cheng, A., Wong, S. M., and Yuan, Y. A. (2009) *Cell Res.* **19,** 187–195
24. Frias-Staheli, N., Giannakopoulos, N. V., Kikkert, M., Taylor, S. L., Bridgen, A., Paragas, J., Richt, J. A., Rowland, R. R., Schmaljohn, C. S., Lenschow, D. J., Snijder, E. J., García-Sastre, A., and Virgin, H. W., 4th (2007) *Cell Host Microbe* **2,** 404–416
25. Akutsu, M., Ye, Y., Virdee, S., Chin, J. W., and Komander, D. (2011) *Proc. Natl. Acad. Sci. U.S.A.* **108,** 2228–2233
26. James, T. W., Frias-Staheli, N., Bacik, J. P., Levingston Macleod, J. M., Khajehpour, M., García-Sastre, A., and Mark, B. L. (2011) *Proc. Natl. Acad. Sci. U.S.A.* **108,** 2222–2227